Talanta 99 (2012) 433–440

Contents lists available at SciVerse ScienceDirect

Talanta

journal homepage: www.elsevier.com/locate/talanta

A fiber-optic sensor to detect volatile organic compounds based on a porous silica xerogel film

Jesús C. Echeverría *, Pablo de Vicente, Juncal Estella, Julián J. Garrido

Departamento de Química Aplicada, Universidad Pública de Navarra, Campus Arrosadía, 31006 Pamplona, Spain

ARTICLE INFO

Article history:
Received 9 January 2012
Received in revised form
1 June 2012
Accepted 4 June 2012
Available online 9 June 2012

Keywords:
Volatile organic compounds
Fiber-optic sensor
Silica xerogel film
Energy of adsorption
Time response curves

ABSTRACT

Fiber-optic sensors are increasingly used for the determination of volatile organic compounds (VOCs) in air matrices. This paper provides experimental results on the sensitivity of a fiber-optic sensor that uses a film of a porous silica xerogel as the sensing element. This film was synthesized by the sol–gel process and affixed to the end of the optical fiber by the dip-coating technique. This intrinsic sensor works in reflection mode, and the transduction takes place in the light that travels through the core of the fiber. The VOCs included in this research cover a wide range of compounds with different functional groups and polarities. The highest sensitivity was for 2-propanol ($13.1 \pm 1.4\ M^{-1}\ nm^{-1}$), followed by toluene ($11.4 \pm 1.4\ M^{-1}\ nm^{-1}$), and 1-butylamine ($9.5 \pm 0.4\ M^{-1}\ nm^{-1}$). Acetone and cyclohexane had the lowest sensitivity of all studied VOCs. Limits of detection varied between 9.1×10^{-5} M for 1-butylamine and 1.6×10^{-3} M for ethanol. Silanol groups on the xerogel surface act as weak acids and interact strongly with molecules that contain OH groups like alcohols, π-electrons like toluene, or a lone pair of electrons like toluene. Stronger interaction of methanol and ethanol with the silanol groups on the film led to some irreversible adsorption of these analytes at room temperature.

1. Introduction

Many scientists worldwide, active in different disciplines such as (i) food, flavor and fragrances, (ii) medical, pharmaceutical and forensic sciences, and particularly (iii) environmental sciences, are concerned about volatile organic compounds (VOCs) [1]. The concern about VOCs arises mainly because of the growing awareness of the impact of VOCs on both human health and the global environment. Both VOCs and their degradation products may contribute to the occurrence of respiratory disorders and cancer [1,2]. VOCs also contribute to major environmental problems such as global warming, stratospheric ozone depletion, and photochemical ozone [3].

VOCs cover a broad range of organic compounds including paraffinic, olefinic and aromatic hydrocarbons and various oxygen-, nitrogen-, sulfur-, and halogen-containing molecules [1]. In the literature, a wide range of definitions of VOCs can be found [4]. Considering the environmental effects, the US Environmental Protection Agency (US-EPA) defines VOCs as organic compounds contributing to the creation of photochemical ozone. Considering the vapor pressure, the American Society for Testing and Materials defines VOCs as organic compounds having a vapor pressure larger than 13.3 Pa at 298 K (Test Method D3960). The European Union Directive for Solvents (1999/13/EC) defines VOCs as organic compounds having a vapor pressure of at least 10 Pa at 293 K.

Most common analytical methods for the determination of VOCs in air and water matrices range from field versions of standard analytical instruments like gas chromatographs with ionization detectors to low-cost alternatives like immunoassay kits. In environmental matrices, where concentrations of VOCs range from pg L^{-1} to μg L^{-1}, appropriate sampling and preconcentration techniques are required because of the sensitivity of the analytical instrument. Some of these approaches still rely on manual collection of samples, so repeated operations are required to determine temporal changes in the hydrocarbon content. Fiber-optic sensors are increasingly used to determine temporal changes in VOCs [2]. The choice of optical fiber technology combined with optoelectronic methodologies and techniques provides several advantages for the achievement of advanced performance in the monitoring system [3,5]. Optical fiber chemical sensors (OFCSs) have some distinctive characteristics. The small size and flexibility of the sensor design makes them ideal tools for in situ and in vivo analysis. Optical fiber sensors are particularly suitable for monitoring various environmental hazards, including either hostile or relatively inaccessible environments. Optical fibers are relatively insensitive to sources of noise, such as electric fields, and signals acquired with optical fibers are much less prone to environmental interferences than signals transmitted through electrical wires. Optical fibers are able to channel a high density of information such as

* Corresponding author. Tel.: +34 948168967; fax: +34 948169006.
E-mail address: jesus.echeverria@unavarra.es (J.C. Echeverría).

0039-9140/$ - see front matter © 2012 Elsevier B.V. All rights reserved.
http://dx.doi.org/10.1016/j.talanta.2012.06.007

wavelength, polarization, and phase. The ability to analyze each of these parameters enhances both the quality and quantity of chemical information obtained by OFCSs.

Porous silica materials synthesized by the sol–gel process combine several physical and chemical properties appropriate to the preparation of optical fiber sensors, such as chemical and thermal stability, inert nature and transparency over a wide range of wavelengths. The textural properties can be tuned by proper selection of the parameters of synthesis including the pH, temperature, water:precursor:solvent molar ratio, and drying conditions [6,7]. The films are usually prepared by spin- or dip-coating from homogeneous colloidal suspensions obtained before the gel point. Thin films require only small amounts of precursors, can embed functional molecules, exhibit fast response times, and are less susceptible to cracking than monoliths.

In a previous study, we developed a fiber-optic sensor with a porous silica xerogel film synthesized by the sol–gel process as the sensing element and evaluated the response to water vapor with a novel measuring cell that works under static volumetric conditions, without interference from atmospheric gases or vapors [8]. This sensor is reversible, capable of sensing relative humidity values as low as 4%, and has response times between 10 s and 2 min, depending on the relative humidity percentage and the measurement procedure.

Other authors have used porous silica and alkyl- or phenyl-modified porous silica as cladding for optical fibers and have tested for the presence of alkanes, hydrocarbons and aromatic compounds [2,9,10]. In these works, volatile organic compounds were diluted in dehydrated air, which acted as carrier gas, and all the measurements were performed at atmospheric pressure. Detection limits for aromatic and alkane analytes with an optical fiber coated with porous silica varied from 6×10^{-3}% (v/v) for xylene to 2.8×10^{-1}% for propane. Silica xerogels have also been used as support matrices for active compounds able to detect VOCs [11–16].

The aim of this research was to assess the sensitivity toward volatile organic compounds of the fiber-optic sensing element that uses a porous silica xerogel synthesized by the sol–gel process as the sensing element, which was already used to detect water vapor [8]. The specific goals were to obtain the time response curves and to evaluate the sensitivity, reproducibility and reversibility of the sensor. The VOCs included in this research cover a wide range of compounds with different functional groups and polarities. We included two hydrocarbons, toluene and cyclohexane. Although both compounds are cyclic compounds, toluene has an aromatic ring with π electrons whereas cyclohexane does not have an aromatic system. The halogenated compounds included are dichloromethane, trichloromethane, and carbon tetrachloride. The selection of these compounds permits the evaluation of the response of the sensing element to variation in the substituent number. A variation in the number of substituents in the molecule affects the size, vapor pressure and polarizability of the molecule. The group of alcohols includes methanol, ethanol and 2-propanol to allow evaluation of the effect of the length of the alkyl chain in addition to the –OH functional group. Acetone is a compound of intermediate polarity, lying between that of alcohols and hydrocarbons. Acetone can also act as a weak electron donor because of the carbonyl group with a pair on non-binding electrons. 1-Butylamine provides the opportunity to study the effect of the nucleophilic amine group on the response.

2. Experimental

2.1. Xerogel film preparation

A multimode optical fiber was chosen with core and cladding diameters of 62.5 and 125 μm, respectively (Telnet, Zaragoza, Spain). The effective refractive index was 1.497 at 850 nm. The fiber was first cut and peeled with a stripper (Millar, Cromwell, CT, USA); then the core and cladding at the end of the fiber were cut with a precision fiber cleaver (Fujikura, Mod. CT-30, Vista, CA, USA).

The xerogel film preparation was performed by the sol–gel process. The silicon alkoxide precursor tetraethylorthosilicate (TEOS) was obtained from Aldrich (Steinheim, Germany) with purity greater than 98%. Hydrochloric acid and absolute ethanol for analysis were supplied by Merck (Darmstadt, Germany), and the water was of MilliQ quality. All chemicals were used without further purification. Ethanol and TEOS were mixed in a 4.75:1 M ratio with continuous stirring. Water was then added dropwise to achieve a 5.5:1 H_2O to TEOS molar ratio. The pH of the solution was adjusted to 4.5 by the addition of HCl with an automated buret (Titrino 702 SM, Metrohm, Herisau, Switzerland) [15,16]. After approximately 4 h of shaking at 333 K, before the gel point occurred at 5 h for this material, the tip of the fiber was dipped into the sol, immersed for 10 seconds and was pulled out at a constant speed of 20 cm min^{-1}. The fiber was then dried for 1 week under atmospheric conditions (atmospheric pressure and 296 ± 2 K) to create a layer of xerogel. The film thickness was about 1.5 μm and was estimated from the FESEM micrograph of fiber tip cross-section [8]. Infrared spectroscopy of the xerogel revealed that the most intense peaks belong to different vibrational modes of a Si–O–Si bonding network, which were centered at 1090, 800, and 400 cm^{-1}. The presence of silanol groups forming H-bonding was confirmed by the presence of a broad adsorption band near 3400 cm^{-1} [6].

2.2. Immersion enthalpy of VOCs on the xerogel

Immersion calorimetry is an experimental technique that may be used to gain information of the interaction energy between the xerogel and the VOCs. When a previously degassed solid is immersed into a liquid in which it does not dissolve or react, it releases some amount of energy known as enthalpy of immersion ($\Delta_{imm}H$) [17,18]. Provided that the solid is previously degassed under vacuum, the enthalpy of immersion mainly depends on the surface area accessible to the liquid, the porous texture of the solid including pore size and shape, the size of the liquid molecules, as well as on the chemical nature of the liquid–solid system [19]. When the enthalpy values are divided into the corresponding BET surface area, the enthalpy of immersion per unit area is obtained.

Immersion enthalpy was obtained with a calorimeter Calvet (Mod. C80, Setaram, Caluire, France). Samples were placed in glass bulbs with a brittle end and they were degassed under vacuum (≤0.1 mbar) at 423 K for 4 h. The bulbs were then sealed, introduced into the calorimeter cell containing 7 cm^3 of the wetting liquid and carefully sealed by o-ring seals. The whole system was placed into the calorimeter block and time was allowed for temperature equilibration between the sample setup and the calorimeter. Once the thermal equilibrium was achieved at 308 K, the brittle end of the bulb was broken so that the liquid entered the bulb and wetted the sample. Heat changes were monitored as a function of time. Integration of heat changes gives the total experimental heat of immersion. Terms, such as exothermic energy of bulb breaking and heat of vaporization of the immersion liquid to fill the empty volume of the bulb with the vapor at the corresponding pressure, were corrected using an empty bulb in parallel.

2.3. Experimental setup

The experimental setup shown in Fig. 1 comprised an optical system, a measuring cell, a vacuum and dosing system, and controllers for temperature and pressure. The optical system

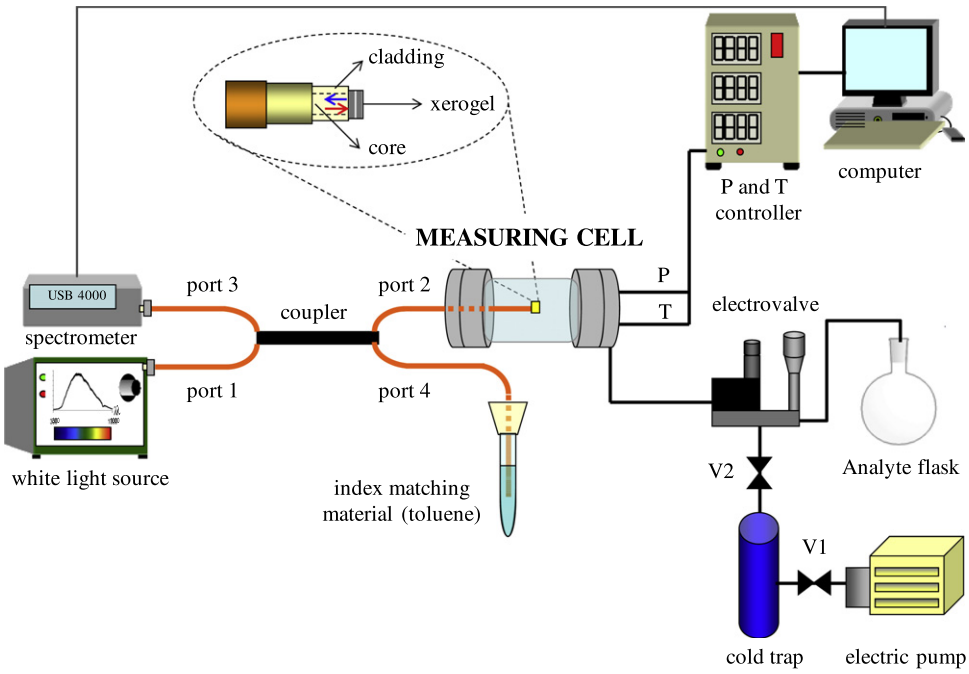

Fig. 1. Experimental setup for registering the sensor response.

included a 50/50 coupler with a 62.5 μm core diameter connected to a white light source (DH-2000, Mikropack) (port 1), the fiber-optic sensor working in reflection mode (port 2), a spectrometer (USB 4000, Ocean Optics (port 3), and a glass tube with toluene as the index matching liquid (port 4). The light signal coming from port 1 is bifurcated into ports 2 and 4. The power light at port 4 is then guided towards the index matching liquid (toluene), where no reflection occurs, to avoid interference, while the signal in port 2 reaches the fiber–xerogel film interface. Exposure of the xerogel film to the analyte vapor inside the measuring cell produces variations in the reflected signal, which is bifurcated back to the coupler and measured at the spectrometer (port 3). The response was as follows:

$$\text{Respone} = \lg\frac{(I_{0(\lambda)}-I_{D(\lambda)})}{(I_{0(\lambda)}-I_{D(\lambda)})} \quad (1)$$

where $I_{0(\lambda)}$ is the optical power monitored from the reference signal, $I_{D(\lambda)}$ is the optical power of the dark reference signal or dark noise and $I_{(\lambda)}$ is the optical power received from the sample, all at a given wavelength range. The dark and reference signal were first registered with the sensing element inside the evacuated measuring chamber.

The measuring cell is a glass cylinder with an isothermal jacket made from the same material and sealed by two Teflon caps, each with different entries. An electronic controller activates the electric valve, which dispenses the analyte vapor inside the measuring cell. The pressure can be fixed either by the controller or by the PXR-LITE software (Tecnomet, Llanera, Spain) in the computer with an error of ± 1 mbar. When the pressure is fixed, the controller sends electric signals to the valve, opening or closing it depending on the programmed pressure. When the level of the pressure sensor corresponds to the programmed level, the controller closes the valve.

2.4. Measuring procedure

After evacuating the measuring chamber to less than 10^{-1} mbar, the pressure was increased to a predetermined value, and, after signal stabilization, the measuring chamber was again evacuated to achieve the initial pressure. We obtained measurements at different pressures, and we registered three cycles with each measurement. Working under volumetric static conditions and assuming ideal behavior, the analyte vapor concentration (c) in the measuring cell is related to the vapor pressure (P) by the equation

$$c = \frac{P}{RT} \quad (2)$$

where R is the gas constant and T is the temperature in Kelvin.

3. Sensing mechanism

The sensing mechanism is based on the change in reflected optical power when molecules are adsorbed on the silica xerogel film. The relative reflected power in an interface between two media depends on the refractive index of the media, the incidence angle, and the polarization of the incident wave. When light impinges perpendicularly to the interface, the reflected optical power between two media of refractive indices n_1 and n_2 is

$$I = \left(\frac{n_2-n_1}{n_2+n_1}\right)^2 I_0 \quad (3)$$

where I is the optical power received from the sample, and I_0 is the optical power monitored from the reference signal. A silica xerogel film coating the tip of the optical fiber acts as an optical cavity where the fiber–xerogel gives the first interface, and the xerogel–vapor gives the second interface. Reflectance of this sensing element may be expressed as follows [20–22]:

$$R = |r|^2 = \frac{r_{12}^2+r_{23}^2+2r_{12}r_{23}\cos 2\beta}{1+r_{12}^2r_{23}^2+2r_{12}r_{23}\cos 2\beta} \quad (4)$$

with

$$r_{12} = \frac{n_{eff}-n_{film}}{n_{eff}+n_{film}}, \quad r_{23} = \frac{n_{film}-n_{ext}}{n_{film}+n_{ext}}, \quad \beta = \left(\frac{4\cdot\pi}{\lambda}\right)\cdot n_{film}\cdot d \quad (5)$$

where coefficients r_{12} and r_{23} are the reflectivity at the fiber–xerogel and xerogel–vapor interfaces, respectively; n_{eff} is the

effective refractive index of the fundamental mode of the optical fiber, n_{film} is the refractive index of the film, n_{ext} is the refractive index of the external medium, λ is the optical wavelength, and d is the film thickness. According to Eqs. (4) and (5), variation in the refractive index of the xerogel and the external medium will lead to changes in the reflectance at the fiber–film interface and, therefore, in the sensor output signal. Changes in the film thickness will also lead to changes in the reflectance at the fiber–film and film–external medium interfaces.

The generation of a signal can be analyzed in terms of two conceptual steps [9]. The first step depends upon the interactions that take place between the analyte and the porous silica. In the second step, the change in the reflected optical power is related to several factors: (1) modification of the refractive index in the interface film–analyte, (2) variation in the real or imaginary component of the refractive index because of interferences, (3) variation in the absorbance caused by the retention of the analyte on the film, and (4) dimensional variation of the film as a consequence of expansion or contraction in the presence of the analyte.

4. Results and discussion

4.1. Time response curves

The analysis temperature was 296 ± 2 K. The wavelength range used to integrate the signal was chosen to optimize the signal to noise ratio. For the sake of clarity, the response is represented on the main y-axis and the pressure on the secondary y-axis. The response was normalized by dividing the change into the wavelength range of integration. We performed three cycles at each prefixed pressure. The prefixed pressure at each step was achieved in approximately 30 s and then stabilized in each measuring step. This time is governed mainly by the step-by-step electric valve mechanism of the dosing system. The response time of the system was defined as t_{90}, the time taken to achieve 90% of the signal change as the environment switches from vacuum to the prefixed pressure and vice versa [23]. From the three measurements at each pressure we obtained the mean, the standard deviation, and the coefficient of variation (CV). In general, the coefficient of variation increased as the analyte concentration and the slope of the regression line decreased. CV ranged from 1% for CH_2Cl_2 concentration higher than 9 mM, to more than 50% for methanol concentration lower than 1.6 mM.

4.1.1. Toluene and cyclohexane

Fig. 2 shows the response of the sensing element in the presence of (a) toluene and (b) cyclohexane. The signal was obtained by integrating the reflected optical power in the range of 800–850 nm for toluene and in the range of 810–850 for cyclohexane. For both compounds, pressure cycles were reproducible, and the prefixed pressure was reached in less than 200 s, although the time depended on the pressure magnitude because the limiting step was the vaporization of analyte inside the flask. The response of toluene and cyclohexane can be characterized by a fast increase of $\lg(I_0/I)$ due to a pressure increase, followed by a slow decrease of the signal to a steady state value. The normalized response was eleven times larger for toluene than for cyclohexane. Toluene showed reproducible cycles between 40 and 5 hPa with a maximum value of 2.0×10^{-2} nm^{-1}. The response of the sensing element in the presence of cyclohexane had a maximum value of approximately 4.0×10^{-3} nm^{-1} for an average pressure of 100 hPa and decreased with the pressure in the range of 100–70 hPa. For pressure values equal to or lower than 60 hPa, the signal variation was concealed by the noise. The baseline drifted toward negative values of $\lg(I_0/I)$ and was more marked for cyclohexane than for toluene.

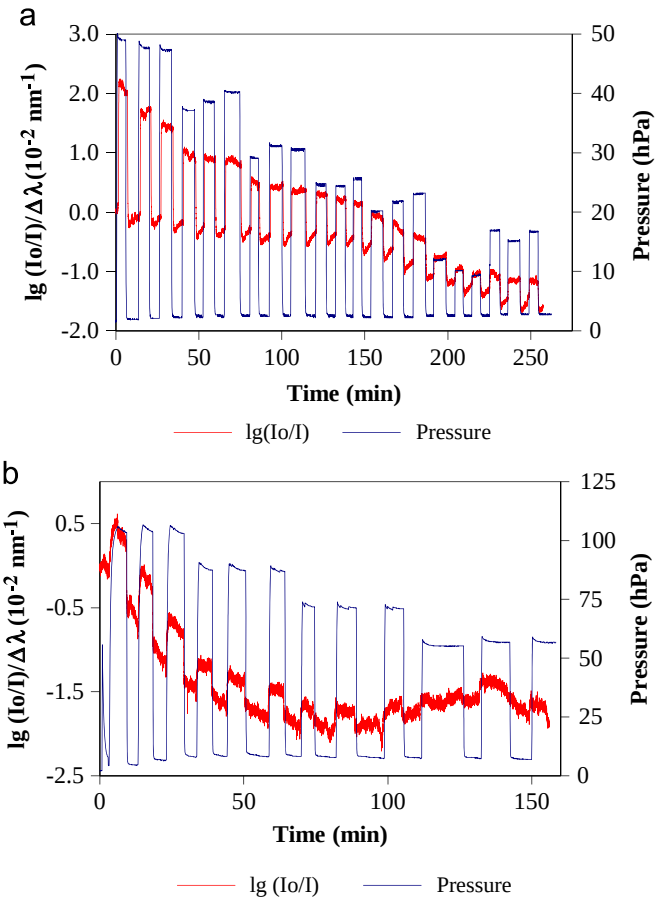

Fig. 2. Time response curves for hydrocarbons: (a) toluene and (b) cyclohexane.

The fact that the response drifted toward negative values indicates that the optical power that reaches the detector is larger than the signal taken as reference with the evacuated measuring chamber. This drift has been attributed to dimensional changes of the film, but another plausible explanation would be related to changes in the refractive indexes in the interfaces fiber–film and film–analyte. The total reflectance is a complex function of the reflectivity on each interface. Assuming that the fiber has an effective refractive index of 1.497, the film an index of 1.402 and the vapor in the chamber an index of 1.00, the reflectivity in the interface fiber–film is 0.069 and in the interface film–analyte 0.169 (Eq. (5)). When the analyte is adsorbed by the film, the reflectivity in the interface film–analyte will decrease because the refractive index for the analyte cannot be assumed to be 1.00, as the reflectivity was when the analyte was a vapor. As a consequence, the reflectivity in the interface film–analyte will be lower than 0.169, as in the interface film-vapor. This modification of the reflectivity on the interface film–adsorbed analyte implies that the reflected optical power (I) will decrease and, therefore, $\lg(I_0/I)$ will also decrease. The decrease in the reflected optical power explains the changes in the signal as the pressure changes. However, when the analyte diffuses through the film, this diffusion could result in a decrease in the overall refractive index of the film and, as a consequence, an increase in the reflected optical power, which will result in negative values of $\lg(I_0/I)$. The contribution of the analyte to the change in the refractive index will depend on the magnitude of the adsorption, the diffusion coefficient of the analyte and the refractive index of the film.

4.1.2. Halogenated compounds

Fig. 3 shows the response of the sensing element to (a) dichloromethane (CH_2Cl_2), (b) trichloromethane ($CHCl_3$) and (c) carbon tetrachloride (CCl_4). The response was obtained by integrating the range 630–670 nm for CH_2Cl_2, 780–840 nm for $CHCl_3$ and 750–800 nm for CCl_4. For the three halogenated compounds, the response was coincident with pressure changes in the measuring chamber. For a fixed value, the pressure presented a maximum before stabilizing in approximately 3 min. The effect was more marked for CH_2Cl_2 and $CHCl_3$ than for CCl_4 because of the higher vapor pressure of dichloromethane (475 hPa at 293 K) and its smaller molecular size (0.33 nm). The magnitude of the response was related to the pressure change in the chamber, which is related to the analyte concentration variation. The baseline drifted towards negative values in the presence of CH_2Cl_2 and CCl_4, with a larger effect for dichloromethane. Trichloromethane showed a minimum value for 140 hPa.

4.1.3. Alcohols

Fig. 4 shows the response of the sensing element in the presence of (a) methanol, (b) ethanol and (c) 2-propanol. The response was obtained by integrating the reflectance between 700 and 750 nm for methanol and ethanol and between 800 and 850 nm for 2-propanol. The response followed the pressure changes for the three alcohols, although the signal corresponding to methanol and ethanol did not stabilize after 5 min, which was the prefixed time for each cycle. The baseline for methanol showed steps that could be related to irreversible changes on the film. The response for ethanol followed pressure changes for

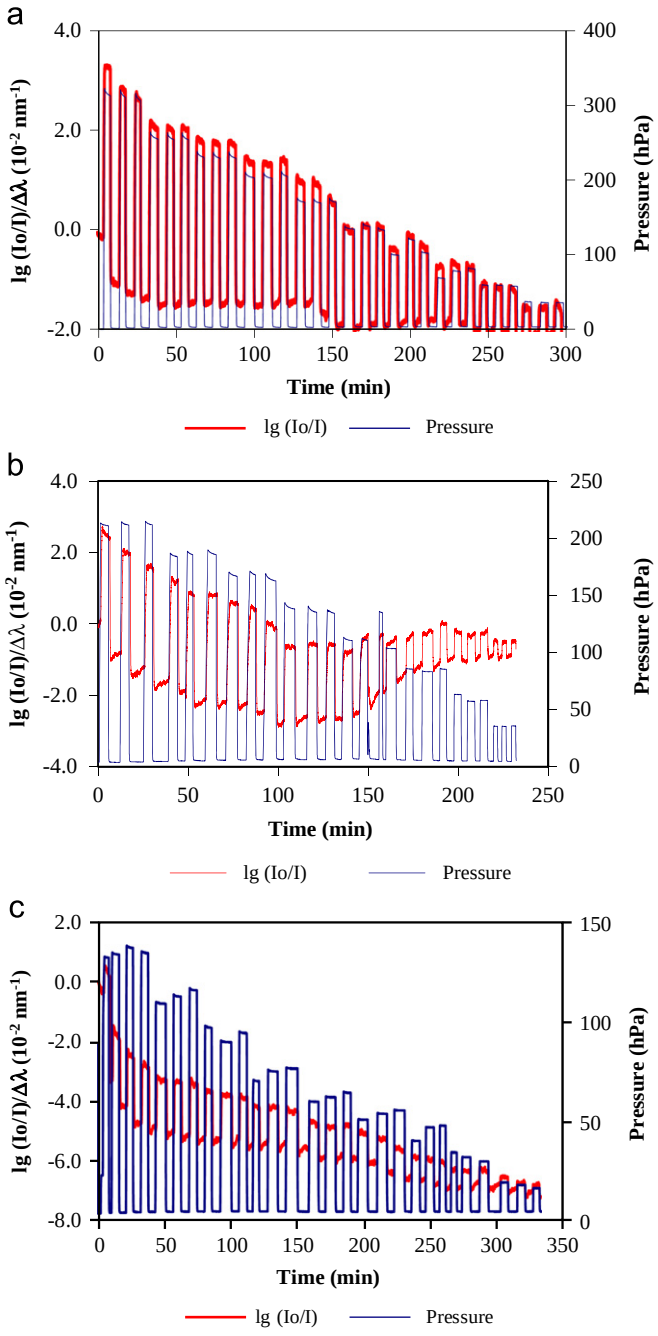

Fig. 3. Time response curves for halogenated hydrocarbons: (a) dichloromethane, (b) trichloromethane, and (c) carbon tetrachloride.

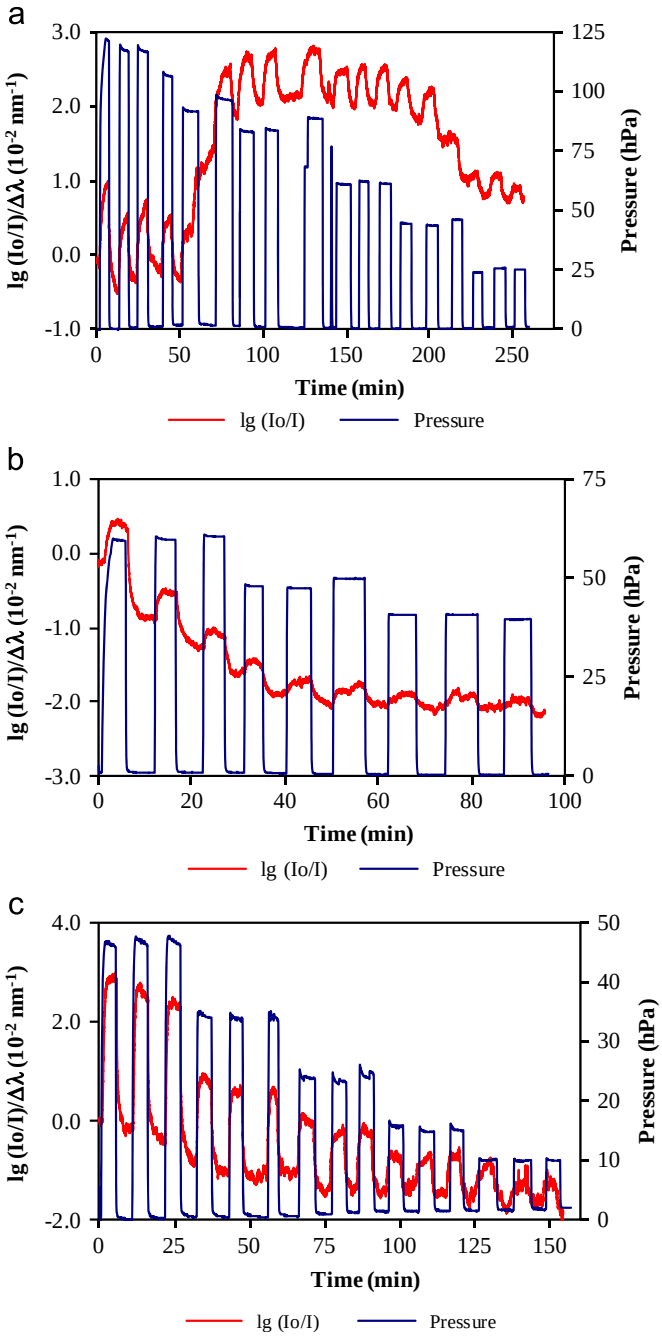

Fig. 4. Time response curves for alcohols: (a) methanol, (b) ethanol, and (c) 2-propanol.

vapor pressures higher than 50 hPa. For values lower than 50 hPa, the signal change was approximately at the level of the baseline noise. When comparing the time response cycles for the three alcohols, 2-propanol presented the best response of the three alcohols in terms of the magnitude of variation, signal stabilization, coefficient of variation, and baseline drift. According to these results, decreasing the polarity of the alcohol improves the response reversibility and the stability of the baseline. For methanol and ethanol, adsorption–desorption processes require a long time, and the baseline is unstable.

4.1.4. Acetone

Among the VOCs investigated, acetone has an intermediate polarity. Acetone possesses a carbonyl functional group with a pair of non-binding electrons that can act as a Lewis base. Pressure cycles were reproducible, and pressure stabilization was achieved at approximately 1 min (Fig. 5). The response was obtained by integrating the reflectance between 630 and 670 nm. The response of the sensing element was synchronized with pressure changes but the magnitude of the signal was lower than 1.0×10^{-2} nm^{-1}. The coefficient of variation increased from 5% for 13 hPa to 39% for 2 hPa. Although the baseline drift was less than other analytes in absolute value, the baseline drift was of the same order as the response changes.

4.1.5. 1-Butylamine

Fig. 6 shows the changes of vapor pressure of butylamine inside the chamber as a function of time and the associated variations of reflected optical power registered by the fiber-optic sensor. The response was obtained by signal integration between 800 and 850 nm. The response time t_{90} varied from approximately 120 s for a prefixed pressure of 8 hPa to 180 s for 50 hPa, the lowest and highest pressure values that were applied, respectively. When 1-butylamine vapor is brought into contact with the sensing element, butylamine molecules diffuse into the film and are adsorbed on the xerogel surface to produce an incremental change in the signal. The magnitude of the response change for each step was a function of the pressure variation. When the pressure was decreased, the opposite process took place, 1-butylamine molecules desorbed into the vapor phase and the magnitude of the response decreased. Adsorption of 1-butylamine molecules on the film surface decreased the reflected optical power, and desorption of 1-butylamine increased the reflected optical power.

The baseline drifted towards negative values. When the chamber was degassed from the prefixed pressure to vacuum pressure, $\lg(I_0/I)/\Delta\lambda$ was lower than the value at the beginning of each cycle. Because the reference reflected power, I_0, and the wavelength range were kept constant, the reflected intensity must be larger than the signal obtained from the film under vacuum at the beginning of the experiment. Incomplete desorption cannot explain the baseline drift. If the 1-butylamine molecules remained adsorbed on the film, the drift should be towards positive values. Swelling effects could also explain the baseline drift.

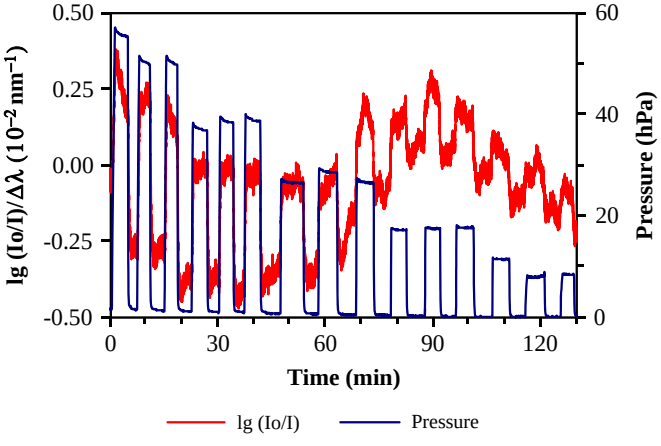

Fig. 5. Time response curve for acetone.

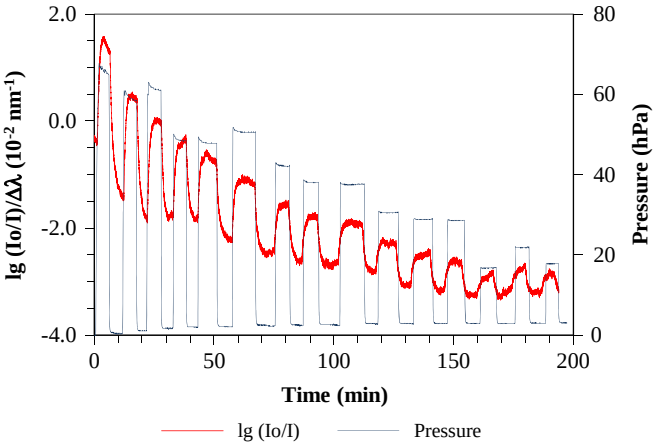

Fig. 6. Time response curve for 1-butylamine.

4.2. Comparison of the response of the sensing element for the selected VOCs

By plotting averaged values of the response as a function of analyte concentration inside the chamber, linear calibration graphs were obtained. Table 1 summarizes the analytical parameters including sensitivity, origin ordinate, quadratic regression coefficient, number of points in the regression line, linear range, and limit of detection. The quadratic regression coefficients were above 0.99 for 2-propanol, toluene, 1-butylamine and halogenated compounds. For the other compounds, quadratic coefficients of regression decreased with the sensitivity of the response. The limits of detection varied from 0.065 mM for 2-propanol to 1.6 mM for ethanol.

Fig. 7 plots the slope of the response for the VOCs in decreasing order. The highest sensitivity was for 2-propanol (13.1 ± 1.4 M^{-1} nm^{-1}), followed by toluene (11.4 ± 1.4 M^{-1} nm^{-1}) and 1-butylamine (9.5 ± 0.4 M^{-1} nm^{-1}). The sensitivities for trichloromethane and carbon tetrachloride were 4.2 ± 0.3 and 4.1 ± 0.1 M^{-1} nm^{-1}, respectively, which were slightly larger than the sensitivity for dichloromethane (3.4 ± 0.1 M^{-1} nm^{-1}). The sensitivities of the alcohols increased with molar mass, but ethanol could not be quantified because confidence limits were larger than the slope. Acetone and cyclohexane had the lowest slopes of all studied VOCs. The slope in the presence of these compounds is approximately twelve times lower than in presence of 2-propanol. As for interferences from the presence of water, this sensor responded reversibly for percentages of relative humidity larger than 4% [8]. Therefore, the presence of water will interfere in the determination of VOCs.

In order to find out trends in the sensitivity of the silica film toward VOCs, we fitted a multiple linear regression model using as the dependent variable the slope of the linear calibration graphs, and as independent variables the refractive index, molar volume, dielectric constant, polarizability, vapor pressure and immersion enthalpy. There was not a statistically significant relationship between the variables at the 95% or higher confidence level, which means that the change in the reflected optical power is a complex process than cannot be attributed to any

Table 1
Analytical parameters calculated from calibration curves: sensitivity, origin ordinate, quadratic regression coefficient (R^2), number of points from the calibration curve (n), linear range (LR), and limit of detection (LOD).

VOC	Sensitivity ($M^{-1}\,nm^{-1}$)	Origin ordinate ($\times 10^{-3}$ (nm^{-1}))	R^2	n	LR (mM)	LOD (mM)
Hydrocarbons						
Toluene	11.4 ± 1.4	5.00 ± 1.60	0.994	6	0.2–0.6	0.26
Cyclohexane	1.0 ± 1.4	-0.8 ± 15.2	0.768	4	ND	ND
Halogenated hydrocarbons						
Dichlormethane	3.4 ± 0.1	-0.4 ± 1.0	0.996	10	0.9–10.0	0.31
Trichloromethane	4.2 ± 0.3	-2.4 ± 2.2	0.992	7	1.4–7.4	0.50
Carbon tetrachloride	4.1 ± 0.1	-0.11 ± 0.8	0.996	7	0.7–3.8	0.18
Alcohols						
Methanol	2.4 ± 0.4	-0.2 ± 1.0	0.987	6	0.7–4.5	0.46
Ethanol	3.4 ± 5.0	4.2 ± 10	0.986	3	1.6–2.3	1.6
2-Propanol	13.1 ± 1.4	1.1 ± 1	0.999	4	0.2–1.2	0.065
Ketones						
Acetone	1.4 ± 0.4	0.2 ± 0.6	0.982	5	0.5–2.2	0.35
Amines						
1-Butylamine	9.5 ± 0.4	-2.2 ± 0.6	0.999	4	0.8–2.0	0.091

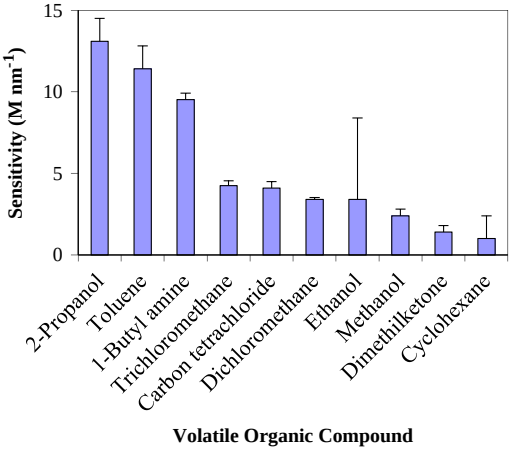

Fig. 7. Sensitivity of the response for the detection of volatile organic compounds with an optical fiber coated with porous silica xerogel.

single factor included in the multiple regression model. However, the fact that the largest response was for 2-propanol, toluene, and 1-butylamine can be explained in terms of the interaction of these compounds with silanol groups on the xerogel film. This xerogel was synthesized at pH 4.5 and has hydrogen-bonded silanol groups on the surface, as demonstrated by a broad band in the 3650–3200 cm^{-1} region of FTIR spectra [6,8,24]. Silanol groups on the surface act as weak acids and interact strongly with molecules that contain OH groups like alcohols through hydrogen bonding, with molecules with π-electrons like toluene, or a lone pair of electrons like 1-butylamine. Both toluene and cyclohexane are cyclic compounds. The immersion enthalpy was –86 mJ m^{-2} for toluene and –37 mJ m^{-2} for cyclohexane. The difference in the immersion enthalpy of these compounds is due to the stronger interaction of silanol groups with the phenyl group of toluene than the interaction with the alicyclic hydrocarbon. Non-specific interactions between cyclohexane and silica are not strong enough to produce a signal larger than the experimental noise. 1-Butylamine, like primary amines, can act as proton acceptor and proton donor in hydrogen bonding. The immersion enthalpy was –236 mJ m^{-2}.

The silica xerogel showed more sensitivity for 2-propanol than for methanol or ethanol. Methanol, ethanol, and 2-propanol adsorb in silica via formation of strong hydrogen bonds. The overall interaction enthalpy obtained by immersion calorimetry was -222 mJ m^{-2} for ethanol, -184 mJ m^{-2} for methanol, and -150 mJ m^{-2} for 2-propanol. Natal-Santiago and Dumesic reported that differential heat curves suggest the existence of at least two adsorption modes of methanol and ethanol coverage [25]. The heat of methanol and ethanol adsorption decreases with coverage, but the ethanol curve passes through a local maximum related to the onset of lateral hydrogen-bonding interactions between neighboring alcohol molecules. Adsorbed methanol can be removed completely from silica by evacuation at 473 K, whereas ethoxy species remain on the oxide surface after evacuation at 573 K. In both cases, the stronger interaction of methanol and ethanol with the silanol groups on the film may lead to some irreversible adsorption of these analytes at room temperature.

Differences in the slope of halogenated compounds were smaller than differences in immersion enthalpy of these compounds, which varied from -62 mJ m^{-2} for carbon tetrachloride to -108 mJ m^{-2} for dichloromethane. The sensitivity for halogenated hydrocarbons was between toluene and cyclohexane, which suggest that the interaction of the phenyl group is larger than the interaction of polarizable molecules such as chlorinated hydrocarbons.

5. Conclusion

The response of the sensing element developed with a porous silica xerogel film covering the tip of a fiber-optic element in the presence of volatile organic compounds is a complex process. With this configuration, the highest sensitivity was obtained with VOCs able to interact with the silica xerogel through hydrogen bonding, like 2-propanol ($13.1 \pm 1.4\,M^{-1}\,nm^{-1}$); through π-electrons of aromatic molecules, like toluene ($11.4 \pm 1.4\,M^{-1}\,nm^{-1}$); or non-binding electrons, such as 1-butylamine ($9.5 \pm 0.4\,M^{-1}\,nm^{-1}$). The response of cyclohexane is ruled by non-specific or van der Waals interactions, which are not sufficient to produce a signal significantly different from the experimental noise. Stronger interaction of methanol and ethanol with the silanol groups on the film led to some irreversible adsorption of these analytes at room temperature. Limits of detection varied from 6.5×10^{-5} M for 2-propanol to 1.6×10^{-3} M for ethanol. The coefficient of variation ranged from 1% for dichloromethane concentration higher than 9 mM, to more than 50% for methanol concentrations lower than 1.6 mM.

Acknowledgments

This work was supported by the Spanish "Ministerio de Ciencia e Innovación" (CTQ2005-08099-CO3-02-BQU and CTQ2009-07993). Juncal Estella Redín is thankful to the Universidad Pública de Navarra for a fellowship.

References

[1] K. Demeestere, J. Dewulf, B. De Witte, H. Van Langenhove, J. Chromatgr. A 1153 (2007) 130–144.
[2] K. Cherif, J. Mrazek, S. Hleli, V. Matejec, A. Abdelghani, M. Chomat, N. Jaffrezic-Renault, I. Kasik, Sens. Actuators B 95 (2003) 97–106.
[3] G. Orellana, D. Haigh, Curr. Anal. Chem. 4 (2008) 273–295.
[4] J. Dewulf, H. Van Langenhove, G. Wittmann, Trends Anal. Chem. 21 (2002) 637–646.
[5] W.Q. Cao, Y.X. Duan, Sens. Actuators B 110 (2005) 252–259.
[6] J. Estella, J.C. Echeverria, M. Laguna, J.J. Garrido, J. Non Cryst. Solids 353 (2007) 286–294.
[7] J. Estella, J.C. Echeverria, M. Laguna, J.J. Garrido, Micropor. Mesopor. Mater. 102 (2007) 274–282.
[8] J. Estella, P. de Vicente, J.C. Echeverria, J.J. Garrido, Sens. Actuators B 149 (2010) 122–128.
[9] A. Abdelghani, J.M. Chovelon, N. Jaffrezic-Renault, M. Lacroix, H. Gagnaire, C. Veillas, B. Berkova, M. Chomat, V. Matejec, Sens. Actuators B 44 (1997) 495–498.
[10] F. Abdelmalek, J.M. Chovelon, M. Lacroix, N. Jaffrezic-Renault, V. Matejec, Sens. Actuators B 56 (1999) 234–242.
[11] C. Bariain, I.R. Matias, C. Fdez-Valdivielso, C. Elosua, A. Luquin, J. Garrido, M. Laguna, Sens. Actuators B 108 (2005) 535–541.
[12] C. Elosua, I.R. Matias, C. Bariain, F.J. Arregui, Sensors 6 (2006) 1440–1465.
[13] A. Luquin, C. Elosua, E. Vergara, J. Estella, E. Cerrada, C. Bariain, I.R. Matias, J. Garrido, M. Laguna, Gold Bull. 40 (2007) 225–233.
[14] C. Elosua, C. Bariain, I.R. Matias, F.J. Arregui, A. Luquin, E. Vergara, M. Laguna, Sens. Actuators B 130 (2008) 158–163.
[15] C. Elosua, C. Bariain, I.R. Matias, F.J. Arregui, E. Vergara, M. Laguna, Sens. Actuators B 137 (2009) 139–146.
[16] C. Elosua, C. Bariain, A. Luquin, M. Laguna, I.R. Matias, Sens. Actuators B 157 (2011) 388–394.
[17] M.J. Meziani, J. Zajac, J.-M. Douillard, D.J. Jones, S. Partyka, J. Rozière, J. Colloid Interf. Sci. 233 (2001) 219–226.
[18] V. Médout-Marère, J.-M. Douillard, in: M. Dekker (Ed.), Encyclopedia of Surface and Colloid Science, Marcel Dekker, Inc., 2002, pp. 4878–4891.
[19] F. Rouquerol, J. Rouquerol, K. Sing, Adsorption by Powders and Porous Solids, 1st ed., Academic Press, San Diego, 1999.
[20] M. Born, E. Wolf, Principles of Optics. Electromagnetic Theory of Propagation, Interference and Diffraction of Light, 7th ed., Cambridge University Press, 2005.
[21] M. Pisco, M. Consales, S. Campopiano, R. Viter, V. Smyntyna, M. Giordano, A. Cusano, J. Lightwave Technol. 24 (2006) 5000–5007.
[22] M. Consales, A. Crescitelli, M. Penza, P. Aversa, P.D. Veneri, M. Giordano, A. Cusano, Sens. Actuators B 138 (2009) 351–361.
[23] C. Higgins, D. Wencel, C.S. Burke, B.D. MacCraith, C. McDonagh, Analyst 133 (2008) 241–247.
[24] P. Innocenzi, J. Non Cryst. Solids 316 (2003) 309–319.
[25] M.A. Natal-Santiago, J.A. Dumesic, J. Catal. 175 (1998) 252–268.